

Research note

Inverse propagation in 1.5-dimensional amplitude-versus-offset joint migration inversion

Sun, Yimin; Verschuur, Eric

DOI

[10.1111/1365-2478.13144](https://doi.org/10.1111/1365-2478.13144)

Publication date

2021

Document Version

Final published version

Published in

Geophysical Prospecting

Citation (APA)

Sun, Y., & Verschuur, E. (2021). Research note: Inverse propagation in 1.5-dimensional amplitude-versus-offset joint migration inversion. *Geophysical Prospecting*, 70(1), 222-234. <https://doi.org/10.1111/1365-2478.13144>

Important note

To cite this publication, please use the final published version (if applicable). Please check the document version above.

Copyright

Other than for strictly personal use, it is not permitted to download, forward or distribute the text or part of it, without the consent of the author(s) and/or copyright holder(s), unless the work is under an open content license such as Creative Commons.

Takedown policy

Please contact us and provide details if you believe this document breaches copyrights. We will remove access to the work immediately and investigate your claim.

Research note: Inverse propagation in 1.5-dimensional amplitude-versus-offset joint migration inversion

Yimin Sun^{1*} and Eric Verschuur²

¹Aramco Research Center – Delft, Aramco Europe, Delft, 2628ZD, The Netherlands, and ²Delft University of Technology, Delft, 2600GA, The Netherlands

Received April 2021, revision accepted July 2021

ABSTRACT

The state-of-the-art joint migration inversion faces the so-called amplitude-versus-offset challenge, due to adopting over-simplified one-way propagation, reflection and transmission operators to avoid over-parameterization in the inversion process. To overcome this challenge, we apply joint migration inversion to horizontally layered media (or 1.5-dimensional media) and parameterize the solution space via density and velocity models. In this scenario, one-way propagation, reflection and transmission operators required by the joint migration inversion process can be analytically and correctly derived from the subsurface models, so the amplitude-versus-offset challenge is successfully overcome. We introduce a new concept, which is named ‘inverse propagation’, into our 1.5-dimensional amplitude-versus-offset joint migration inversion. It can correctly reconstruct subsurface wavefields by using a surface-recorded receiver wavefield with all the influence of transmission, reflection and multiples accounted for. A synthetic example is used to demonstrate the correctness of the inverse propagation. This work is the foundation to further develop the 1.5-dimensional amplitude-versus-offset joint migration inversion technology.

Key words: Acoustics, Computing aspects, Full waveform, Modelling, Theory.

INTRODUCTION

As a relatively new technology, joint migration inversion (JMI) is formulated in the acoustic framework and simultaneously deals with velocity model building and seismic imaging (Berkhout, 2014b). JMI belongs to the school of full-waveform inversion (FWI), and it tries to fit forward modelled data with measurements (Verschuur *et al.*, 2016). Many similarities can be found between JMI and imaging-oriented FWI (Kalinicheva *et al.*, 2020; Zhang *et al.*, 2020), reflection FWI (Xu *et al.*, 2013; Valensi *et al.*, 2017; Gisolf *et al.*, 2021) and migration-based traveltime waveform inversion (Clément *et al.*, 2001; Chavent, 2017). JMI aims at exploiting all multiples in data for inversion, and the key is in its unique modelling engine, which is named full wavefield

modelling (FWMod) (Berkhout, 2014a). JMI and FWMod are based upon wavefield separation (Sun and Fei, 2018; Sun and Fei, 2021), and the concrete wavefield separation scheme adopted therein is based on Bremmer’s series using one-way operators (Berkhout, 2014a). JMI parameterizes the subsurface via a migration velocity model and a reflectivity model. Furthermore, it assumes that these two models are decoupled (Berkhout, 2014b; Sun *et al.*, 2020). Although in physics a reflectivity model should be dependent on propagation angles, this in reality creates an enormous solution space for inversion in JMI, which leads to over-parameterization of the inverse problem where many velocity models with suitable angle-dependent reflectivities can fit the data. Consequently, current implementations of JMI adopt over-simplified operators (Sun *et al.*, 2018b): for propagation operators, it uses the local explicit operators (Etgen, 1994); for transmission and reflection operators, it uses angle-independent operators

*Email: sun.delft@gmail.com

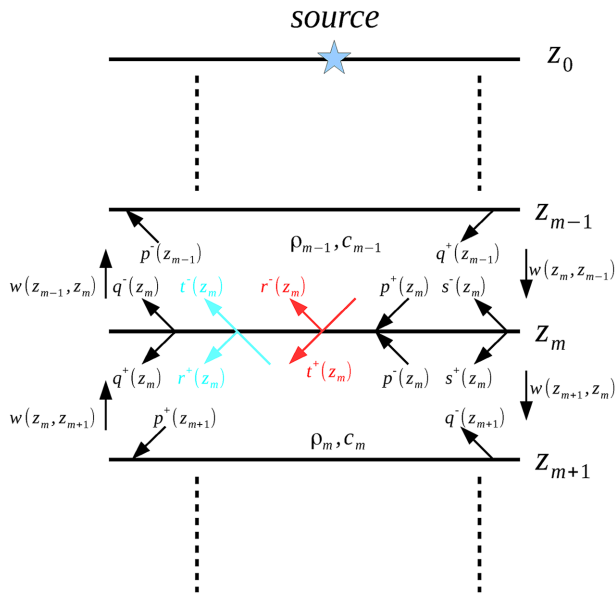


Figure 1 The fundamental wavefield propagation model used in 1.5D-AVO-FWMod and 1.5D-AVO-JMI. Note that all the wavefield-related symbols in this figure are actually subject to a certain combination of k_x and ω . For example, $q^+(z_m)$ actually represents $q^+(z_m; k_x, \omega)$. The symbols shown in this figure are defined as follows: ρ and c are velocity and density of a layer, the superscript + or – represents down-going or up-going propagation, z_m is the depth of the m th interface in the z direction, p is an incoming wavefield, q is an outgoing wavefield, t or r is a transmission or reflection coefficient, s is an injection source wavefield, and w is a one-way propagator.

(Verschuur *et al.*, 2016; Sun *et al.*, 2019). Via a comparison study, we have systematically investigated the influence of these simplified operators on JMI results (Sun *et al.*, 2020), where the amplitude-versus-offset (AVO) challenge has been pointed out for the current JMI. Some initiatives to overcome this AVO challenge for JMI are currently underway (Davydenko and Verschuur, 2017; Qu *et al.*, 2018; Sun and Verschuur, 2020).

In this paper, we propose to apply acoustic JMI to horizontally layered media, which is also commonly named 1.5-dimensional media. Although we still use one-way propagation, reflection and transmission operators to describe wave propagations, we now first parameterize the solution space via a velocity model and a density model, and next use these models to derive all those one-way operators required by JMI. In such a scenario, one-way propagation, reflection and transmission operators can be analytically defined in a physically correct way (Berkhout, 1987), so we naturally overcome the AVO challenge. To avoid confusion, throughout the rest of this paper, we refer to our new variant of JMI by 1.5D-AVO-JMI and refer to the current JMI technology (Berkhout, 2014b) by

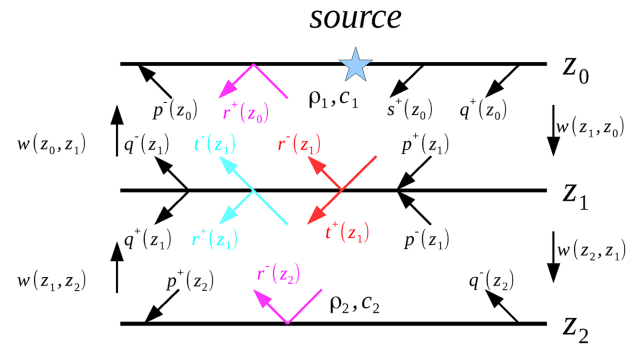


Figure 2 A two-layer model to illustrate the concept of inverse propagation.

the traditional JMI. 1.5D-AVO-JMI should have applications in locally horizontally layered media containing strong multiple generators. We further introduce a new concept named ‘inverse propagation’, which can correctly reconstruct subsurface wavefields required by 1.5D-AVO-JMI using a surface-recorded receiver wavefield and accommodating physical causality effects during the course of wave propagation.

The rest of this paper is organized as follows. We first formulate a detailed theory of 1.5D-AVO-FWMod, which is the modelling engine used in 1.5D-AVO-JMI. We next introduce the ‘inverse propagation’ concept in detail. We further discuss how we deal with the challenge of numerical instability when applying the inverse propagation in reality and use a synthetic example to demonstrate the correctness of the ‘inverse propagation’ concept.

1.5-DIMENSIONAL AMPLITUDE-VERSUS-OFFSET FULL WAVEFIELD MODELLING

Our theories for both 1.5D-AVO-FWMod and 1.5D-AVO-JMI are derived in the temporal frequency–spatial wavenumber domain. We consider a pressure signal corresponding to a combination of k_x and ω , where k_x is a spatial wavenumber in the x direction and ω is an angular frequency. Our theories are acoustic, and thus the 1.5-dimensional (1.5D) media are isotropic. Under these considerations, we can set spatial wavenumbers in the y direction to zeros, that is, $k_y = 0$, as long as we make sure to have sufficient sampling for k_x . As a result, for a temporal frequency f and a medium with a velocity c , the relationships connecting spatial wavenumbers k_x and k_z with a corresponding wavenumber k are

$$\omega = 2\pi f, \quad k = \frac{\omega}{c}, \quad k_x^2 + k_z^2 = k^2. \quad (1)$$

The wavefield propagation model in both 1.5D-AVO-FWMod and 1.5D-AVO-JMI is shown in Figure 1, which

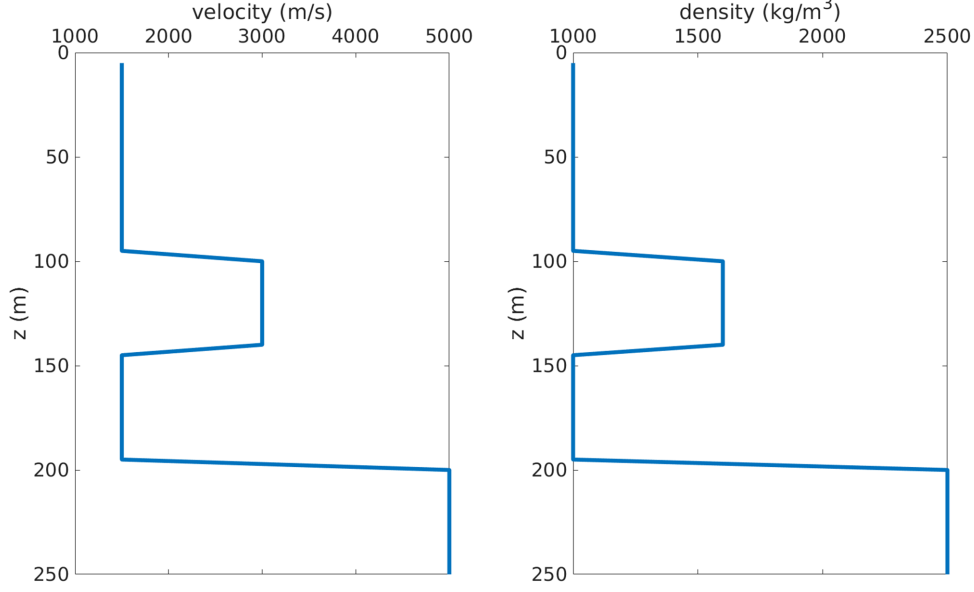


Figure 3 The true 1.5D model.

is similar to that in the traditional joint migration inversion (JMI) (Sun *et al.*, 2019). Note that all the wavefield-related symbols in Figure 1 are actually scalars subject to a certain combination of k_x and ω , as there exist no physically non-linear effects, such as frequency conversion, in our wavefield propagation theory. In other words, both the spatial and the temporal frequencies are decoupled, and thus wave propagation equations can be written independently for different combinations of k_x and ω . For example, $q^+(z_m)$ there actually represents $q^+(z_m; k_x, \omega)$. The symbols shown in Figure 1 are defined as follows: ρ and c are velocity and density of a layer, the superscript + or - represents down-going or up-going propagation, z_m is the depth of the m th interface in the z direction, p is an incoming wavefield, q is an outgoing wavefield, t or r is a transmission or reflection coefficient, s is an injection source wavefield, and w is a one-way propagator. In 1.5D media, $w(z_m, z_{m+1})$ and $r^-(z_m)$ have been discussed before (Berkhout, 1987; Sun *et al.*, 2018a) and they can be written as

$$w(z_{m+1}, z_m) = \begin{cases} \exp(-ik_{z,m}|z_{m+1} - z_m|) & \text{if } k_m^2 \geq k_x^2 \\ \exp(-|k_{z,m}| |z_{m+1} - z_m|) & \text{otherwise} \end{cases}, \quad (2)$$

$$r^-(z_m) = \frac{\rho_{m+1}k_{z,m} - \rho_m k_{z,m+1}}{\rho_{m+1}k_{z,m} + \rho_m k_{z,m+1}}, \quad (3)$$

$$k_{z,m} = \sqrt{k_m^2 - k_x^2}, \quad (4)$$

where $k_m = \frac{\omega}{c_m}$.

Similar to full wavefield modelling (FWMOD), 1.5D-AVO-FWMod also engages iterations in its modelling process, and we use n to explicitly denote its modelling iteration: $n = 0$ is the first iteration corresponding to primaries; $n = 1$ is the second iteration corresponding to the first-order multiples; ... Using symbols shown in Figure 1, the theory of 1.5D-AVO-FWMod can be formulated as follows:

$$q_n^+(z_m) = s^+(z_m) + t^+(z_m) p_n^+(z_m) + r^+(z_m) p_{n-1}^-(z_m), \quad (5)$$

$$q_n^-(z_m) = s^-(z_m) + t^-(z_m) p_n^-(z_m) + r^-(z_m) p_n^+(z_m), \quad (6)$$

$$p_n^+(z_m) = w(z_m, z_{m-1}) q_n^+(z_{m-1}), \quad (7)$$

$$p_n^-(z_m) = w(z_m, z_{m+1}) q_n^-(z_{m+1}), \quad (8)$$

$$r^-(z_m) = -r^+(z_m), \quad (9)$$

$$t^+(z_m) = 1 + r^-(z_m), \quad (10)$$

$$t^-(z_m) = 1 + r^+(z_m), \quad (11)$$

$$w(z_m, z_{m+1}) = w(z_{m+1}, z_m), \quad (12)$$

where n is the multiple order (or the iteration order). Note that $p_{-1}^-(z_m) = 0$ in equation (5).

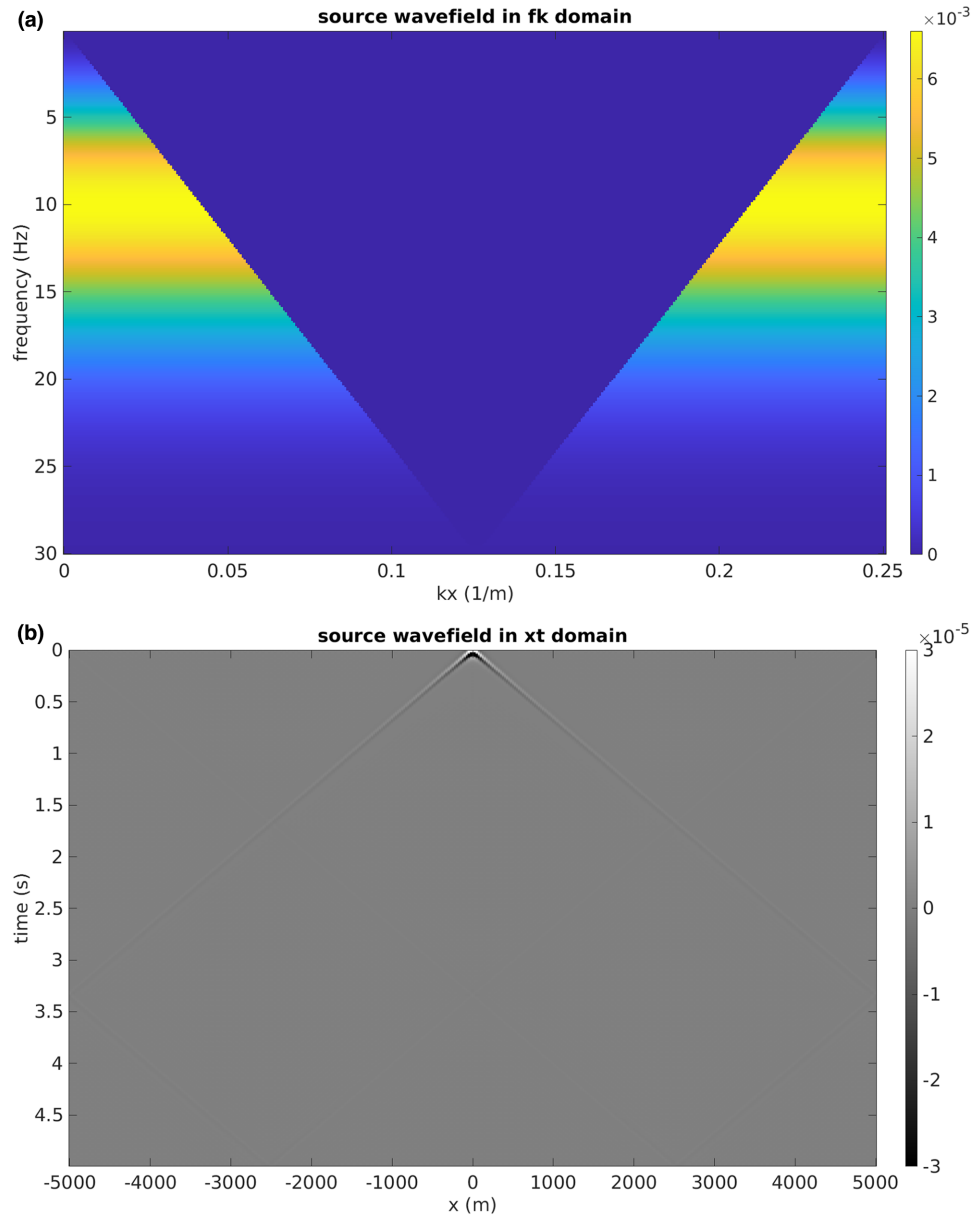


Figure 4 (a) The amplitude spectrum of the source wavefield in our simulation. (b) The source wavefield is in the x - t domain.

Equations (1)–(12) reflect the philosophy behind Bremmer’s series. Each iteration of 1.5D-AVO-FWMod corresponds to one order of multiples, and it comprises a wavefield propagating from the surface of the model to the bottom reflection interface of the model and then being reflected back to the surface. During the course of one iteration, transmission and reflection effects are accounted for, and contributions from previous iterations, that is, multiples, are also accommodated. The inclusion of surface-related multiples can be explicitly controlled by $q_n^+(z_0)$,

which is the down-going and out-going wavefield at the surface:

$$q_n^+(z_0) = \begin{cases} s^+(z_0) + r^+(z_0) p_{n-1}^-(z_0), & \text{free surface} \\ s^+(z_0), & \text{absorption surface} \end{cases} \quad (13)$$

Although the theory of 1.5D-AVO-FWMod looks similar to that of FWMod (Berkhout, 2014a; Sun *et al.*, 2019) in its formality, there exist fundamental differences:

- The solution space is parameterized via medium parameters ρ and c .

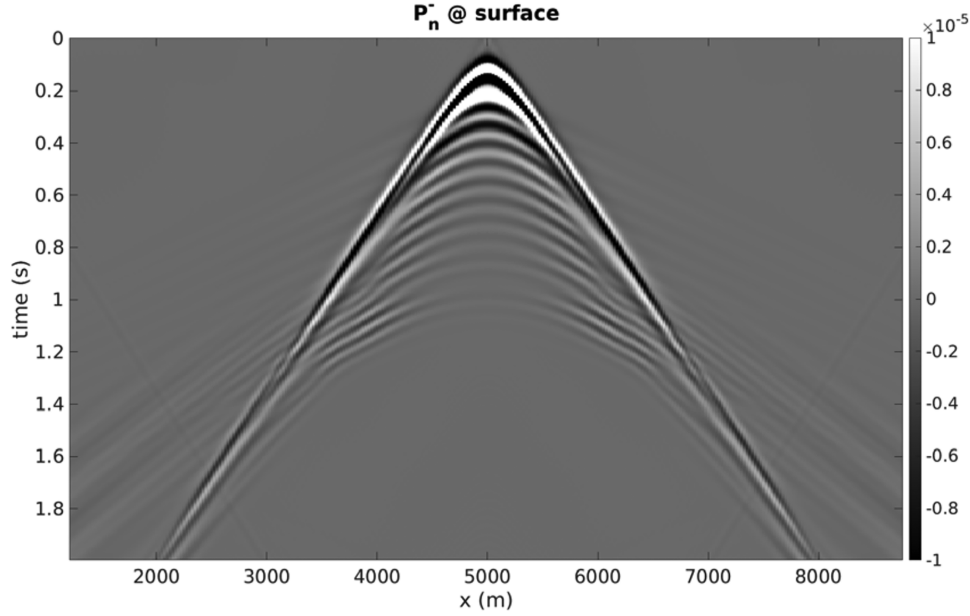


Figure 5 The measured surface wavefield when only considering internal multiples. The maximum multiple order is 10.

- Transmission and reflection effects can now be physically accounted for via equations (3) and (9)–(11), and hence the amplitude-versus-offset effect in input data can be correctly simulated.
- All components are separable in the (k_x, ω) domain, and hence we are now dealing with scalar computations. In other words, all symbols in equations (5)–(12) are scalars.

In seismic data acquisition, usually sources are located at the surface. Furthermore, we normally estimate a source wavefield that only contains downward propagating components. So throughout this paper, we set the below requirements to the source terms in equations (5) and (6):

$$s^-(z_m) = 0 \text{ for all } z_m, \quad (14)$$

$$s^+(z_m) = 0 \text{ for } z_m \neq z_0. \quad (15)$$

Note the traditional JMI (Berkhout, 2014b; Verschuur *et al.*, 2016; Sun *et al.*, 2019, 2020) adopts conditions similar to equations (14) and (15).

INVERSE PROPAGATION IN 1.5-DIMENSIONAL AMPLITUDE-VERSUS-OFFSET JOINT MIGRATION INVERSION

In the traditional joint migration inversion (JMI), a crucial component is to use a receiver wavefield recorded at the surface to reconstruct proper subsurface wavefields for the

purpose of gradient calculations. Reconstructing subsurface wavefields is not a trivial task as it is highly non-linear and engages effects of physical causality. The backward propagation scheme is the engine for reconstructing these subsurface wavefields in the traditional JMI, but this scheme only considers dealing with the propagation effect and the transmission effect (Staal, 2015; Sun *et al.*, 2019). We hereby propose a new concept that is named ‘inverse propagation’ for surface-recorded receiver wavefields. It aims at correctly addressing the effects of propagation, transmission, reflection and physical causality to reconstruct proper subsurface wavefields from a surface receiver wavefield for 1.5D-AVO-JMI.

In order to understand why we introduce this new concept of inverse propagation to 1.5D-AVO-JMI, we use a two-layer model, shown in Figure 2, to demonstrate the limitations of the backward propagation scheme used in the traditional JMI. We first use the primaries, that is, the first iteration of 1.5D-AVO-FWMod, as an example, and its complete simulation process is as follows:

$$q_0^+(z_0) = s^+(z_0), \quad (16)$$

$$p_0^+(z_1) = w(z_1, z_0) q_0^+(z_0), \quad (17)$$

$$q_0^+(z_1) = t^+(z_1) p_0^+(z_1), \quad (18)$$

$$p_0^+(z_2) = w(z_2, z_1) q_0^+(z_1), \quad (19)$$

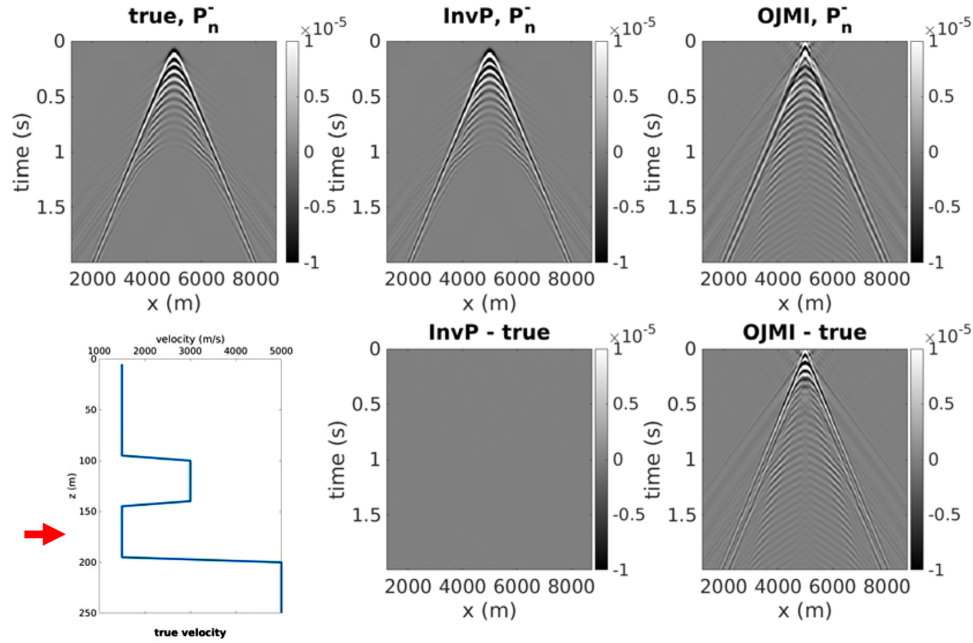


Figure 6 The situation when only internal multiples are considered and the maximum multiple order is 10. (Top left) The ground truth of the up-going and incoming wavefield p_n^- at $z = 175$ m. (Top middle) The reconstructed up-going and incoming wavefield \tilde{p}_n^- at $z = 175$ m via the inverse propagation of the surface wavefield $p_n^-(0)$. (Top right) The reconstructed up-going and incoming wavefield \tilde{p}_n^- at $z = 175$ m via the backward propagation scheme used in the traditional JMI (OJMI). (Bottom left) The true 1.5D velocity with the red arrow pointing at the target subsurface interface. (Bottom middle) The difference between the reconstructed wavefield via the inverse propagation and the ground truth. (Bottom right) The difference between the reconstructed wavefield via the backward propagation and the ground truth.

$$q_0^-(z_2) = r^-(z_2) p_0^+(z_2), \quad (20)$$

$$p_0^-(z_1) = w(z_1, z_2) q_0^-(z_2), \quad (21)$$

$$q_0^-(z_1) = t^-(z_1) p_0^-(z_1) + r^-(z_1) p_0^+(z_1), \quad (22)$$

$$p_0^-(z_0) = w(z_0, z_1) q_0^-(z_1). \quad (23)$$

Note that all symbols in equations (16)–(23) are scalars, as already discussed in the previous section.

Starting with the surface-recorded wavefield $p_0^-(z_0)$, the backward propagation scheme (Staal, 2015; Sun *et al.*, 2019) reconstructs the wavefields $\tilde{q}_0^-(z_1)$ and $\tilde{p}_0^-(z_1)$ as follows:

$$\begin{aligned} \tilde{q}_0^-(z_1) &= w(z_0, z_1)^{-1} p_0^-(z_0) = w(z_0, z_1)^{-1} w(z_0, z_1) \\ q_0^-(z_1) &= q_0^-(z_1), \end{aligned} \quad (24)$$

$$\begin{aligned} \tilde{p}_0^-(z_1) &= t^-(z_1)^{-1} \tilde{q}_0^-(z_1) = t^-(z_1)^{-1} \\ &[t^-(z_1) p_0^-(z_1) + r^-(z_1) p_0^+(z_1)] \\ &= p_0^-(z_1) + t^-(z_1)^{-1} r^-(z_1) p_0^+(z_1). \end{aligned} \quad (25)$$

Comparing equations (24) and (25) to equations (22) and (21), we can clearly see that although the backward propagation scheme in the traditional JMI can correctly deal with the propagation effect, it violates the causality of forward wavefield propagation by incorrectly introducing the term $t^-(z_1)^{-1} r^-(z_1) p_0^+(z_1)$ into the reconstructed wavefield $\tilde{p}_0^-(z_1)$.

We next use a total wavefield containing both primaries and the first order of multiples, that is, to run two iterations of 1.5D-AVO-FWMod, from this two-layer model to further demonstrate this causality effect in the backward propagation scheme of the traditional JMI. Iteration 2 of 1.5D-AVO-FWMod follows equations (16)–(23) as shown below:

$$q_1^+(z_0) = s^+(z_0) + r^+(z_0) p_0^-(z_0), \quad (26)$$

$$p_1^+(z_1) = w(z_1, z_0) q_1^+(z_0), \quad (27)$$

$$q_1^+(z_1) = t^+(z_1) p_1^+(z_1) + r^+(z_1) p_0^-(z_1), \quad (28)$$

$$p_1^+(z_2) = w(z_2, z_1) q_1^+(z_1), \quad (29)$$

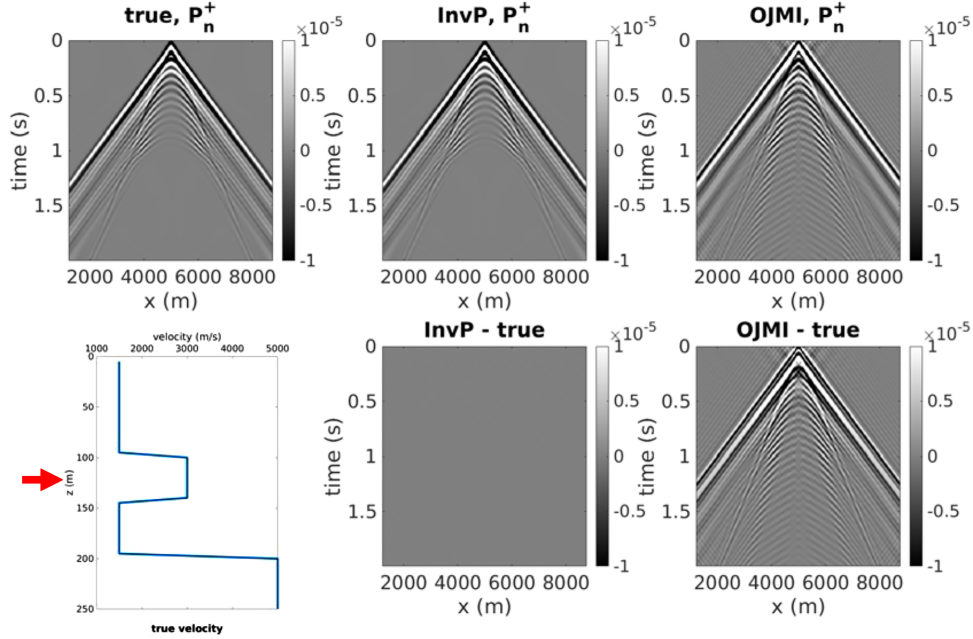


Figure 7 The situation when only internal multiples are considered, and the maximum multiple order is 10. (Top left) The ground truth of the down-going and incoming wavefield p_n^+ at $z = 125$ m. (Top middle) The reconstructed down-going and incoming wavefield \tilde{p}_n^+ at $z = 125$ m via the inverse propagation of the surface wavefield $p_n^-(0)$. (Top right) The reconstructed down-going and incoming wavefield \tilde{p}_n^+ at $z = 125$ m via the backward propagation scheme used in the traditional JMI (OJMI). (Bottom left) The true 1.5D velocity with the red arrow pointing at the target subsurface interface. (Bottom middle) The difference between the reconstructed wavefield via the inverse propagation and the ground truth. (Bottom right) The difference between the reconstructed wavefield via the backward propagation and the ground truth.

$$q_1^-(z_2) = r^-(z_2) p_1^+(z_2), \quad (30)$$

$$p_1^-(z_1) = w(z_1, z_2) q_1^-(z_2), \quad (31)$$

$$q_1^-(z_1) = t^-(z_1) p_1^-(z_1) + r^-(z_1) p_1^+(z_1), \quad (32)$$

$$p_1^-(z_0) = w(z_0, z_1) q_1^-(z_1). \quad (33)$$

If we use the backward propagation scheme in the traditional JMI with the measured surface wavefield $p_1^-(z_0)$, that is, equation (33), we can get the reconstructed wavefields $\tilde{q}_1^-(z_1)$ and $\tilde{p}_1^-(z_1)$ as follows:

$$\begin{aligned} \tilde{q}_1^-(z_1) &= w(z_0, z_1)^{-1} p_1^-(z_0) = w(z_0, z_1)^{-1} w(z_0, z_1) \\ & q_1^-(z_1) = q_1^-(z_1), \end{aligned} \quad (34)$$

$$\begin{aligned} \tilde{p}_1^-(z_1) &= t^-(z_1)^{-1} \tilde{q}_1^-(z_1) = t^-(z_1)^{-1} \\ & [t^-(z_1) p_1^-(z_1) + r^-(z_1) p_1^+(z_1)] \\ & = p_1^-(z_1) + t^-(z_1)^{-1} r^-(z_1) p_1^+(z_1). \end{aligned} \quad (35)$$

Similar to the conclusions reached about equations (24) and (25), we can see that although the backward propagation scheme can correctly deal with the propagation effect, it violates the causality by incorrectly introducing the term $t^-(z_1)^{-1} r^-(z_1) p_1^+(z_1)$ into the reconstructed wavefield $\tilde{p}_1^-(z_1)$.

We now introduce the inverse propagation scheme, which can correctly account for this causality influence, in a general situation. We first consider reconstructing up-going wavefields from a surface receiver wavefield $p_n^-(z_0)$. According to equation (8), the up-going and out-going wavefield $\tilde{q}_n^-(z_m)$ can be computed as

$$\tilde{q}_n^-(z_m) = w(z_{m-1}, z_m)^{-1} \tilde{p}_n^-(z_{m-1}), \quad (36)$$

where $\tilde{p}_n^-(z_{m-1})$ is the reconstructed up-going and incoming wavefield at $z = z_{m-1}$.

At the surface, that is $z = z_0$, we have a particular relationship for the $\tilde{p}_n^-(z_0)$:

$$\tilde{p}_n^-(z_0) = p_n^-(z_0). \quad (37)$$

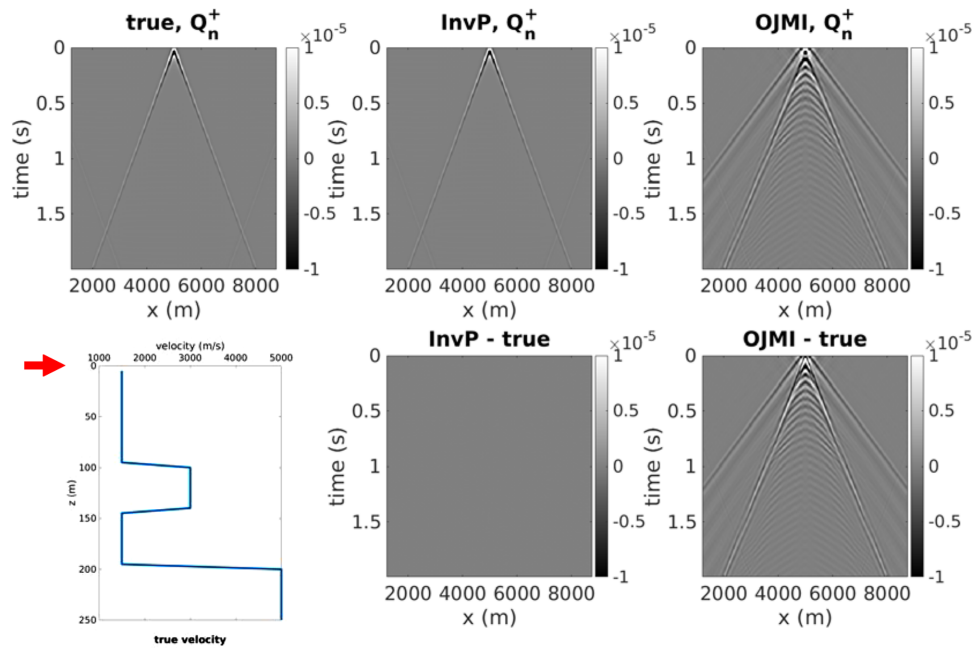


Figure 8 The situation when only internal multiples are considered, and the maximum multiple order is 10. (Top left) The ground truth of the down-going and outgoing wavefield q_{n-1}^+ at $z = 0$ m, the surface. (Top middle) The reconstructed down-going and incoming wavefield \widehat{q}_{n-1}^+ at $z = 0$ m via the inverse propagation of the surface wavefield $p_n^-(0)$. (Top right) The reconstructed down-going and incoming wavefield \widehat{q}_{n-1}^+ at $z = 0$ m via the backward propagation scheme used in the traditional JMI (OJMI). (Bottom left) The true 1.5D velocity with the red arrow pointing at the target subsurface interface. (Bottom middle) The difference between the reconstructed wavefield via the inverse propagation and the ground truth. (Bottom right) The difference between the reconstructed wavefield via the backward propagation and the ground truth.

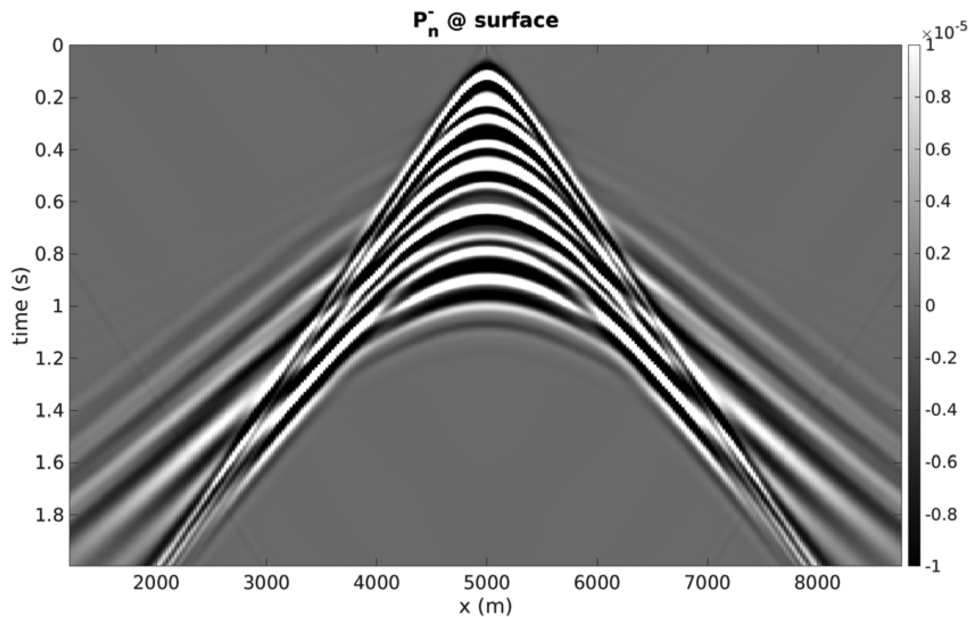


Figure 9 The measured surface wavefield when considering both surface and internal multiples. The maximum multiple order is 5.

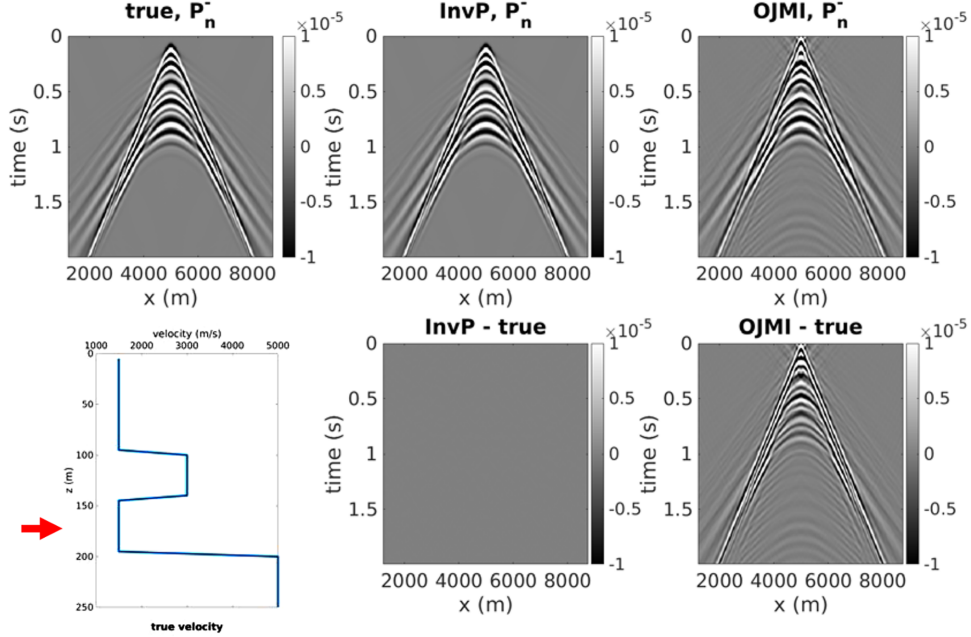


Figure 10 The situation when both surface and internal multiples are considered, and the maximum multiple order is 5. (Top left) The ground truth of the up-going and incoming wavefield $\widetilde{p}_n^-(z_m)$ at $z = 175$ m. (Top middle) The reconstructed up-going and incoming wavefield \widetilde{p}_n^- at $z = 175$ m via the inverse propagation of the surface wavefield $p_n^-(0)$. (Top right) The reconstructed up-going and incoming wavefield \widetilde{p}_n^- at $z = 175$ m via the backward propagation scheme used in the traditional JMI (OJMI). (Bottom left) The true 1.5D velocity with the red arrow pointing at the target subsurface interface. (Bottom middle) The difference between the reconstructed wavefield via the inverse propagation and the ground truth. (Bottom right) The difference between the reconstructed wavefield via the backward propagation and the ground truth.

According to equations (6), (14) and (15), $\widetilde{p}_n^-(z_m)$ where $m > 0$ can be reconstructed by

$$\widetilde{p}_n^-(z_m) = t^-(z_m)^{-1} \widetilde{q}_n^-(z_m) - t^-(z_m)^{-1} r^-(z_m) p_n^+(z_m), \quad (38)$$

where the term $p_n^+(z_m)$ is obtained via a forward simulation using 1.5D-AVO-FWMod, that is, through equations (1)–(13) with a source wavefield and subsurface models provided by users as the input. We name the term ‘ $-t^-(z_m)^{-1} r^-(z_m) p_n^+(z_m)$ ’ a compensation term. It bears the causality effect on the reconstruction of $\widetilde{p}_n^-(z_m)$ from the surface wavefield $p_n^-(z_0)$, and it has to be accounted for in order to correctly reconstruct $\widetilde{p}_n^-(z_m)$. Although the traditional JMI ignores this causality effect in its backward propagation scheme (Berkhout, 2014b; Vershuur *et al.*, 2016; Sun *et al.*, 2019, 2020), this compensation term now is a key component in the inverse propagation scheme of 1.5D-AVO-JMI. Note that Berkhout (2014a) does describe a different way of inverse full wavefield modelling, which is via subtraction of the scattering term at each depth level. However, this cannot provide a direct estimate of the up-going wavefield as shown in equation (38).

At the bottom reflection interface, that is, $z = z_{\max}$, according to equation (6), we can retrieve the inversely propagated down-going and incoming wavefield $\widetilde{p}_n^+(z_m)$ by

$$\widetilde{p}_n^+(z_{\max}) = r^-(z_{\max})^{-1} \widetilde{q}_n^-(z_{\max}). \quad (39)$$

Note here we adopt the condition $p_n^-(z_{\max}) = 0$, as we are now considering the bottom reflection interface.

With $\widetilde{p}_n^+(z_{\max})$ being available from equation (39), we can further recursively reconstruct the down-going and outgoing (or incoming) wavefield $\widetilde{q}_n^+(z_m)$ (or $\widetilde{p}_n^+(z_m)$). According to equations (7) and (5), they can be calculated as

$$\widetilde{q}_n^+(z_m) = w(z_{m+1}, z_m)^{-1} \widetilde{p}_n^+(z_{m+1}), \quad (40)$$

$$\widetilde{p}_n^-(z_m) = t^+(z_m)^{-1} \widetilde{q}_n^+(z_m) - t^+(z_m)^{-1} r^+(z_m) p_{n-1}^-(z_m). \quad (41)$$

Similar to equation (38), the term ‘ $-t^+(z_m)^{-1} r^+(z_m) p_{n-1}^-(z_m)$ ’ is also a compensation term addressing the causality effect, and $p_{n-1}^-(z_m)$ has to be obtained via a forward simulation using 1.5D-AVO-FWMod.

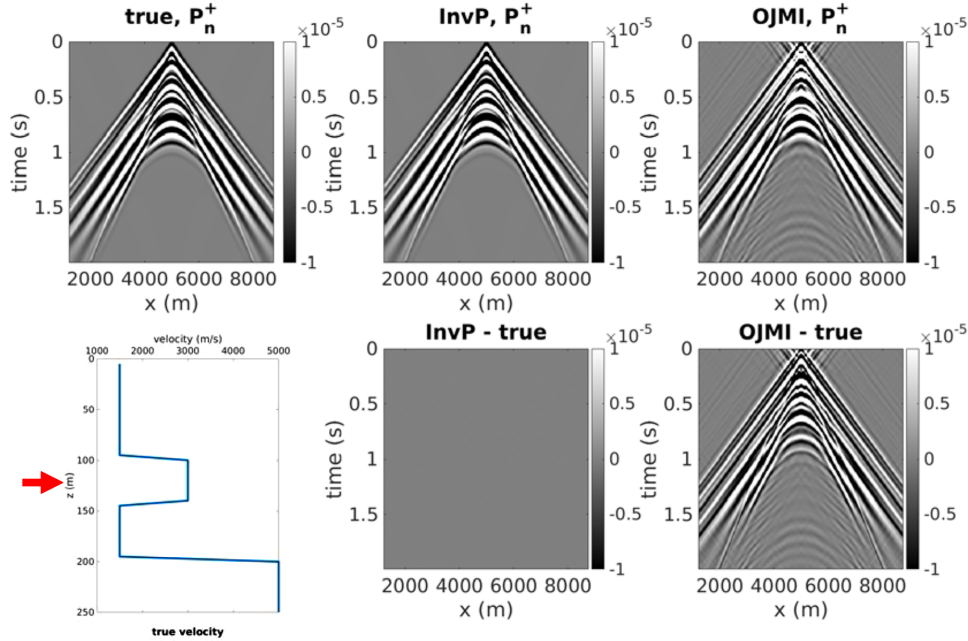


Figure 11 The situation when both surface and internal multiples are considered, and the maximum multiple order is 5. (Top left) The ground truth of the down-going and incoming wavefield p_n^+ at $z = 125$ m. (Top middle) The reconstructed down-going and incoming wavefield \tilde{p}_n^+ at $z = 125$ m via the inverse propagation of the surface wavefield $p_n^-(0)$. (Top right) The reconstructed down-going and incoming wavefield \tilde{p}_n^+ at $z = 125$ m via the backward propagation scheme used in the traditional JMI (OJMI). (Bottom left) The true 1.5D velocity with the red arrow pointing at the target subsurface interface. (Bottom middle) The difference between the reconstructed wavefield via the inverse propagation and the ground truth. (Bottom right) The difference between the reconstructed wavefield via the backward propagation and the ground truth.

Equations (36)–(41) form the complete theory of inverse propagation in 1.5D-AVO-JMI. Via the compensation terms, the inverse propagation correctly accounts for the influence of propagation, transmission, reflection and multiples to reconstruct subsurface wavefields using a surface receiver wavefield. However, in order to obtain the compensation terms, we need to run 1.5D-AVO-FWMod for the required $p_n^+(z_m)$ and $p_{n-1}^-(z_m)$ in Equations (38) and (41).

Before wrapping up this section, we would like to emphasize again that our inverse propagation scheme differs from the backward propagation scheme in the traditional JMI in the compensation terms. The compensation terms reflect causality, and they account for influences of transmission, reflection and multiples.

NUMERICAL STABILITY

The inverse propagation introduced above, that is, equations (36)–(41), is a recursive process, and it engages many inverse calculations, including $w(z_{m+1}, z_m)^{-1}$, $t^-(z_m)^{-1}$, $t^+(z_m)^{-1}$ and $r^-(z_{\max})^{-1}$. Note that all these symbols are scalars in 1.5D-AVO-JMI, as already explained earlier in this paper. In prac-

tice, this poses a severe challenge for the numerical stability. As far as we know, there are two ways to overcome this challenge. The first way is to resort to high-precision arithmetic libraries, for instance, Multiple Precision Toolbox for MATLAB (Barrowes, 2020) and The GNU Multiple Precision Floating-Point Reliable Library (GNU MPFR) (Fousse *et al.*, 2005). The other way, which we believe is a more practical solution and thus is adopted in this paper, is a phase-guided solution. Details of this phase-guided algorithm can be found in Oppenheim and Lim (1981) and Bakulin *et al.* (2020). In this section, we briefly introduce how we use this algorithm to stabilize our numerical calculations in the inverse propagation scheme.

As introduced above, in the inverse propagation of 1.5D-AVO-JMI, we need to do forward simulation to get $p_n^+(z_m)$ and $p_{n-1}^-(z_m)$ for compensation terms. To stabilize the calculation, we also use the corresponding forward-simulated wavefield amplitudes as the amplitudes of reconstructed wavefields. In other words, in our example, equations (36)–(41) are implemented as follows:

$$\begin{aligned} \tilde{q}_n^-(z_m) &= w(z_{m-1}, z_m)^{-1} \tilde{p}_n^-(z_{m-1}) \\ &|w(z_{m-1}, z_m)^{-1} \tilde{p}_n^-(z_{m-1})|^{-1} |q_n^-(z_m)|, \end{aligned} \quad (42)$$

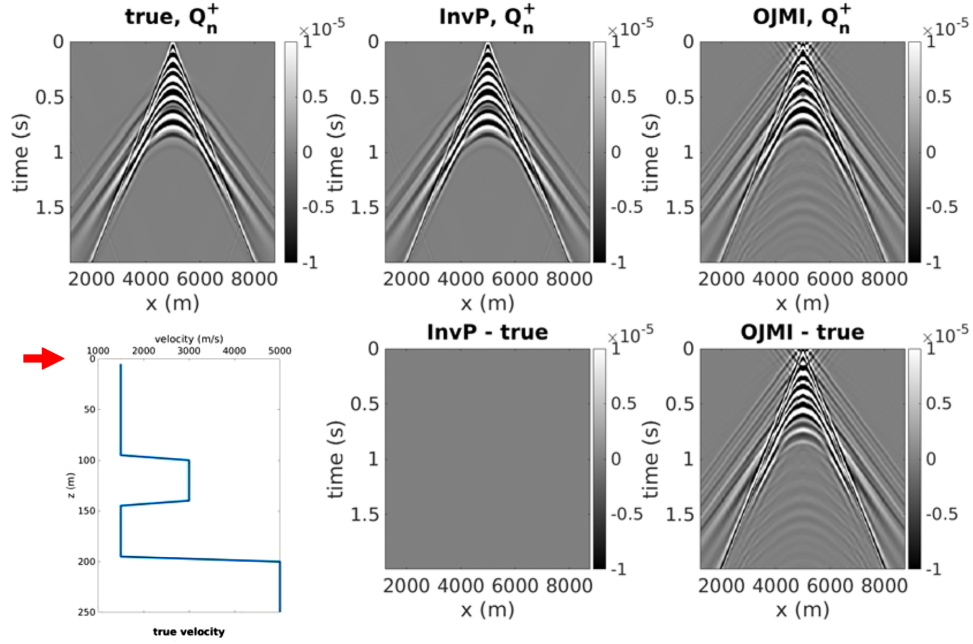


Figure 12 The situation when both surface and internal multiples are considered and the maximum multiple order is 5. (Top left) The ground truth of the down-going and outgoing wavefield q_{n-1}^+ at $z = 0$ m, the surface. (Top middle) The reconstructed down-going and incoming wavefield \widetilde{q}_{n-1}^+ at $z = 0$ m via the inverse propagation of the surface wavefield $p_n^-(0)$. (Top right) The reconstructed down-going and incoming wavefield \widetilde{q}_{n-1}^+ at $z = 0$ m via the backward propagation scheme used in the traditional JMI (OJMI). (Bottom left) The true 1.5D velocity with the red arrow pointing at the target subsurface interface. (Bottom middle) The difference between the reconstructed wavefield via the inverse propagation and the ground truth. (Bottom right) The difference between the reconstructed wavefield via the backward propagation and the ground truth.

$$\begin{aligned} \widetilde{p}_n^-(z_m) &= \left[t^-(z_m)^{-1} \widetilde{q}_n^-(z_m) - t^-(z_m)^{-1} r^-(z_m) p_n^+(z_m) \right] \\ &\quad \left| t^-(z_m)^{-1} \widetilde{q}_n^-(z_m) - t^-(z_m)^{-1} r^-(z_m) p_n^+(z_m) \right|^{-1} \\ &\quad \left| p_n^-(z_m) \right|, \end{aligned} \quad (43)$$

$$\begin{aligned} \widetilde{p}_n^+(z_{max}) &= r^-(z_{max})^{-1} \widetilde{q}_n^-(z_{max}) \left| r^-(z_{max})^{-1} \widetilde{q}_n^-(z_{max}) \right|^{-1} \\ &\quad \left| p_n^+(z_{max}) \right|, \end{aligned} \quad (44)$$

$$\begin{aligned} \widetilde{q}_n^+(z_m) &= w(z_{m+1}, z_m)^{-1} \widetilde{p}_n^+(z_{m+1}) \\ &\quad \left| w(z_{m+1}, z_m)^{-1} \widetilde{p}_n^+(z_{m+1}) \right|^{-1} \left| q_n^+(z_m) \right|, \end{aligned} \quad (45)$$

$$\begin{aligned} \widetilde{p}_n^+(z_m) &= \left[t^+(z_m)^{-1} \widetilde{q}_n^+(z_m) - t^+(z_m)^{-1} r^+(z_m) p_{n-1}^-(z_m) \right] \\ &\quad \left| t^+(z_m)^{-1} \widetilde{q}_n^+(z_m) - t^+(z_m)^{-1} r^+(z_m) p_{n-1}^-(z_m) \right|^{-1} \\ &\quad \left| p_n^+(z_m) \right|, \end{aligned} \quad (46)$$

where $|a|$ means taking the amplitude of the input variable a . Note that all demonstrations in the Example section use equations (42)–(46) for the inverse propagation.

Before wrapping up this section, we would like to point out that our phase-guided solution requires a good estimation of the input source wavelet for forward simulation. Detailed discussion on retrieving a high-fidelity source wavelet from raw seismic data is beyond the scope of this paper, and interested readers can refer to Verschuur *et al.* (1989), Carvalho and Weglein (1994) and Matson (2000) for some technical details.

EXAMPLE

We use a 1.5-dimensional (1.5D) synthetic model, shown in Figure 3, to demonstrate the inverse propagation scheme in 1.5D-AVO-JMI. There exist several multiple generators in the subsurface. The source wavefield $s^+(z_0)$ in our demonstration is shown in Figure 4 in both the frequency–spatial wavenumber domain and the x - t domain. Our source wavefield covers a spectrum between 0.2 and 30 Hz. As the purpose of this

paper is to demonstrate the inverse propagation concept in 1.5D-AVO-JMI, the source wavefield is our a priori knowledge. We use the 1.5D-AVO-FWMod as our forward modelling engine, and the data-simulation-related parameters in our example are as follows: both the initial frequency and the frequency step are 0.2 Hz, and the maximum frequency is 30 Hz; the maximum source–receiver offset is 5 km, and the receiver spacing is 25 m; the grid size in the z direction is 5 m.

Figure 5 shows the surface wavefield when only internal multiples are considered in our data, that is, with an absorption surface condition applied. We set the maximum order of internal multiples to 10. Via the inverse propagation scheme, that is, equations (36)–(41) and using the models and the source wavefield shown in Figures 3 and 4 as the input, we reconstruct the up-going and incoming wavefield \widetilde{p}_n^- at $z = 175$ m, the down-going and incoming wavefield \widetilde{p}_n^+ at $z = 125$ m, and the down-going and outgoing wavefield \widetilde{q}_{n-1}^+ at the surface. Our reconstructed wavefields are shown in the top middle pictures in Figures 6–8; the top left pictures in these figures show the ground truth; the top right pictures show the reconstructed wavefields by the backward propagation scheme in the traditional joint migration inversion (we use the traditional joint migration inversion [OJMI] to represent this scheme on a figure); the bottom middle pictures show the difference between the ground truth and the reconstructed wavefields by the inverse propagation; the bottom right pictures show the difference between the ground truth and the reconstructed wavefields by the backward propagation. We can easily observe that our inverse propagation scheme indeed correctly reconstructs all subsurface wavefields when the input models and the source wavefield are correct, while the backward propagation scheme yields inaccuracies. Figure 9 shows the surface wavefield when both surface and internal multiples are considered in our data, that is, with a free surface condition applied. We set the maximum order of multiples to 5 in this example. Comprehensive result comparisons, the same as those shown in Figures 6–8, are shown in Figures 10–12. In this situation, we can also easily observe that our inverse propagation scheme works correctly when the input models and the source wavefield are correct.

CONCLUSIONS

In this paper, we introduce the inverse propagation concept in the 1.5-dimensional amplitude-versus-offset joint migration inversion (1.5D-AVO-JMI). 1.5D-AVO-JMI still uses one-way propagation, transmission and reflection operators to describe

wave propagation, but it first parameterizes the subsurface via a density model and a velocity model and then uses these models to derive the corresponding physical one-way operators. 1.5D-AVO-JMI overcomes the amplitude-versus-offset challenge as now one-way propagation, reflection and transmission operators are physically correct. The inverse propagation concept uses the compensation terms to account for causality effects during the course of wavefield propagation, and it is a theoretically rigorous way to reconstruct subsurface wavefields in 1.5D-AVO-JMI. We also discuss a practical challenge when implementing the inverse propagation in 1.5D-AVO-JMI, which is the numerical stability, and we propose to use the phase-guided algorithm to overcome it. Our synthetic examples corroborate the correctness of our theories. We believe this work can act as the solid theoretical foundation to further develop the 1.5D-AVO-JMI technology.

DATA AVAILABILITY STATEMENT

Research data are not shared.

REFERENCES

- Bakulin, A., Silvestrov, I. and Neklyudov, D. (2020) Importance of phase guides from beamformed data for processing multi-channel data in highly scattering media. *The Journal of the Acoustical Society of America*, 147(6), EL447-EL452.
- Barrowes, B. (2020) Multiple Precision Toolbox for MATLAB. *MATLAB Central File Exchange*. Available at <https://www.mathworks.com/matlabcentral/fileexchange/6446-multiple-precision-toolbox-for-matlab> [Accessed 10 September 2020].
- Berkhout, A.J. (1987) *Applied Seismic Wave Theory*, Volume 1. Elsevier.
- Berkhout, A.J. (2014a) Review paper: An outlook on the future of seismic imaging, Part I: Forward and reverse modelling. *Geophysical Prospecting*, 62, 911–930.
- Berkhout, A.J. (2014b) Review paper: An outlook on the future of seismic imaging, Part III: Joint migration inversion. *Geophysical Prospecting*, 62, 950–971.
- Carvalho, P.M. and Weglein, A.B. (1994) Wavelet estimation for surface multiple attenuation using a simulated annealing algorithm. In: *SEG Expanded Abstracts*. SEG, pp. 1481–1484.
- Clément, F., Chavent, G. and Gómez, S. (2001) Migration-based traveltimes waveform inversion of 2-D simple structures: a synthetic example. *Geophysics*, 66, 845–860.
- Chavent, G. (2017) Data space reflectivity and the migration based travel time approach to FWI. In: *EAGE Extended Abstracts*. EAGE, WS09 A01.
- Davydenko, M. and Verschuur, D.J. (2017) Full-wavefield estimation of angle-dependent reflectivity and migration velocity. In: *SEG Technical Program Expanded Abstracts*. SEG, pp. 5631–5635.

- Etgen, J.T. (1994) Stability of explicit depth extrapolation through laterally-varying media. In: *SEG Expanded Abstracts*. SEG, pp. 1266–1269.
- Fousse, L., Hanrot, G., Lefèvre, V., Pélissier, P. and Zimmermann, P. (2005) MPFR: a multiple-precision binary floating point library with correct rounding. *Research Report*, RR-5753, INRIA, inria-00070266, pp. 15.
- Kalinicheva, T., Warner, M. and Mancini, F. (2020) Full-bandwidth FWI. In: *SEG Expanded Abstracts*. SEG, pp. 651–655.
- Gisolf, A., Haffinger, P.R. and Doulgeris, P. (2021) AVO modeling and interpretation with the help of the 1.5D elastic wave-equation. *First Break*, 39(3), 93–100.
- Matson, K. (2000) An overview of wavelet estimation using free-surface multiple removal. *The Leading Edge*, 19(1), 50–55.
- Oppenheim, A.V. and Lim, J.S. (1981) The importance of phase in signals. *Proceedings of the Institute of Electrical and Electronics Engineers*, 69, 529–541.
- Qu, S., Sun, Y. and Verschuur, E. (2018) Mitigating amplitude versus ray-parameter effect in joint migration inversion using a zero-lag cross-correlation objective function of redatumed wavefields. In: *SEG Technical Program Expanded Abstracts*. SEG, pp. 1133–1137.
- Staal, X. (2015) Combined imaging and velocity estimation by joint migration inversion. *Ph.D. thesis*, Delft University of Technology. Accessed September 13, 2021. Available at <https://repository.tudelft.nl/islandora/object/uuid:f9cfa765-dac4-4954-9b6b-01b8c7345018/?collection=research>.
- Sun, Y., Verschuur, E. and van Borselen, R. (2018a) Acoustic propagation operators for pressure signals on an arbitrarily curved surface in a homogeneous medium. *Journal of Applied Geophysics*, 150, 314–324.
- Sun, Y., Kim, Y.S., Qu, S., Verschuur, E., Almomin, A. and van Borselen, R. (2018b) Joint migration inversion versus FWI-RTM: A comparison study on a 2D realistic deep water model. In: *EAGE Extended Abstract*. EAGE, Th P3 10.
- Sun, Y. and Fei, T.W. (2018) Wavefield separation at an arbitrary propagation direction via FK filtering. In: *SEG Expanded Abstracts*. SEG, pp. 4171–4175.
- Sun, Y., Verschuur, E. and Qu, S. (2019) Research note: Derivations of gradients in angle-independent joint migration inversion. *Geophysical Prospecting*, 67, 572–579.
- Sun, Y., Kim, Y.S., Qu, S. and Verschuur, E. (2020) Joint Migration Inversion: Features and challenges. *The Journal of Geophysics and Engineering*, 17(3), 525–538.
- Sun, Y. and Fei, T.W. (2021) Flank-preserving de-primary reverse time migration. *Geophysics*, 86(1), S1–S15.
- Sun, Y. and Verschuur, E. (2020) Full wavefield modelling using rigorous one-way propagation, reflection and transmission operators. In: *SEG Expanded Abstracts*. SEG, pp. 2694–2698.
- Valensi, R., Baina, R. and Duprat, V. (2017), Reflection waveform inversion method: Solutions to the reflectivity-background coupling problem and consequences on the convergence. In: *79th Annual International Meeting, EAGE, Expanded Abstracts*. EAGE, WS09 D03.
- Verschuur, D.J., Berkhouit, A.J. and Wapenaar, C.P.A. (1989) Wavelet estimation by prestack multiple elimination. In: *SEG Expanded Abstracts*. SEG, pp. 1129–1132.
- Verschuur, D.J., Staal, X.R. and Berkhouit, A.J. (2016), Joint migration inversion: Simultaneous determination of velocity fields and depth images using all orders of scattering. *The Leading Edge*, 35, 1037–1046.
- Xu, S., Chen, F., Lambaré, G. and Zhang, Y. (2013) Full waveform inversion of reflected seismic data. *Journal of Seismic Exploration*, 22(5), 449–462.
- Zhang, Z., Wu, Z., Wei, Z., Mei, J., Huang, R. and Wang, P. (2020) FWI Imaging: Full-wavefield imaging through full-waveform inversion. In: *SEG Expanded Abstracts*. SEG, pp. 656–660.